EasyChair Preprint

№ 8343

Real-Time Localization for Mobile Machines by Fusing Barometric Altitude Measurements with Surface Profiles

Lukas Michiels, Benjamin Kazenwadel, Simon Becker and Marcus Geimer

EasyChair preprints are intended for rapid dissemination of research results and are integrated with the rest of EasyChair.

June 21, 2022

Real-time localization for mobile machines by fusing barometric altitude measurements with surface profiles

Lukas Michiels, Benjamin Kazenwadel, Simon Becker and Marcus Geimer
Institute for Mobile Machines (Mobima)
Karlsruhe Institute of Technology (KIT)
Karlsruhe, Germany
lukas.michiels@kit.edu, benjamin.kazenwadel@kit.edu, simon.becker@kit.edu, marcus.geimer@kit.edu

***Abstract*—Accurate localization is one of the key requirements for the automation of mobile machines. While GNSS-based systems are widely used due to their high accuracy and accessibility, redundant systems have to be developed to decrease the dependency on GNSS signals for autonomous machines. Although altitude measurements have been used for many decades by human explorers, they are not yet exploited for localization purposes on mobile machines. Based on single barometric measurements, no localization is possible as the vehicle could be at various positions with the same absolute altitude. In this paper, we propose an algorithm based on sequential importance sampling to fuse altitude measurements with surface profiles, which allows real-time tracking and localization of mobile machines. When moving through hilly terrain, a machine constantly changes its altitude, and the altitude profile can be used to track the vehicle's position. The proposed algorithm offers a supplementary localization and verification method for mountainous and potentially GNSS-obstructed areas.**

***Index Terms*—Robotics, Nonlinear filtering, Localization, Tracking, Mobile Machines, GNSS, Barometric Measurements, Magnetic Heading, Autonomous Systems**

I. Introduction

Automated agricultural machinery is getting in the focus of research and development since a long time. Innovative control systems and strategies have been developed to increase process efficiency and decrease operating costs. These systems have a high dependency on accurate global positioning, such as the electronic tow bar for agricultural machines, which allows an unmanned tractor to follow a human-operated machine [1]. These systems must be reliable to allow for undisturbed operations without the interference of exterior influences. Today most of the localization is handled using GNSS measurements, based on GPS, GLONASS, Galileo, or Baidou (BDS) satellite data. The GPS accuracy can be enhanced using Real-Time Kinematics (RTK) from static measurement stations for accuracy of up to 2 cm [2].

However, these systems are highly dependent on a continuous connection to as many satellites as possible to ensure the overall accuracy. The accuracy is largely decreased if the antenna is obstructed, for example in forests, where alternative localization systems are a necessity [3]. In addition, GNSS-signals can be easily interfered with jamming and spoofing attacks, proposing a risk if the machine is driving autonomously without an intervening human operator supervising the system. These issues propose the usage of additional sensors for redundancy. Alternative solutions based on odometry data or feature point recognition become increasingly sophisticated in the automotive sector [4], [5]. Meanwhile, off-road applications feature a variety of additional challenges on the localization methods. Missing clear feature points such as roads and traffic symbols and the uneven surface terrain without fixed driving patterns thereby suggest the usage of different methods [6]. The usage of topographical maps for navigation purposes is of historic relevance and used for navigation in mountainous terrain. Map quality has improved with the usage of satellite and plane-based surface measurement technologies in recent years [7], [8]. While the measurement of relative height differences between static objects is easy, absolute altitude measurements for localization in these maps constitute a difficult task if the dependency on exterior signals (e.g. GNSS) should be avoided. The atmospheric pressure measurement grants the necessary independence and is a proven technology with a development time of several centuries [9]. Barometric data is frequently used for altitude estimation in aviation since relative deviations between measurements in different aerial vehicles are robust and can therefore be used to avoid collisions [10]. Absolute height measurements propose additional difficulties due to the influence of the weather on absolute atmospheric pressure levels [11]. This can be avoided when frequently calibrating the measurements devices at a known position or reference data. Nowadays, barometers are widely available, cheap, and accurate [10]. Research has been conducted using barometric data for altitude calculation before the wide availability of satellite data [11], [12]. At the time, the use of barometric measurements was limited to the calculation of vertical distances. Several newer studies fused barometric altitude data with alternative sources. In [13], barometric data was used to create a more accurate altitude estimation compared to a GPS-only based system. They detected the GPS-signal reliability using a Receiver Autonomous Integrity Monitoring (RAIM) algorithm and in the case of a reliable signal, it was merged with the barometric data using an Extended

Kalman Filter (EKF) or a Weighted Least-Square measurement model. Both approaches resulted in an improvement compared to the GPS-only approach. In [14] a merging algorithm for the data from the inertial navigation system of an aircraft was presented. It received GNSS data and barometric data to improve the robustness of altitude measurements against sensor anomalies. They suggest the usage of an EKF for sensor fusion. There have been several efforts to use barometric data for indoor positioning from direct pressure level usage on mobile smartphones [15]–[17]. Similar studies were conducted to assess the possibility of merging barometric data with WiFi- and Bluetooth data or using Inertial Measurement Units (IMU) to detect floor level changes or to fuse the information using an EKF to improve the localization [18]–[22]. In contrary to outdoor applications, these approaches either focus solely on vertical localization or rely on measuring the received signal strength from external senders such as WiFi-antennas for horizontal localization. Land-based outdoor localization cannot rely on these signals and needs therefore different approaches. In [23] fusing barometric data with GNSS and IMU data using an EKF to improve localization quality was investigated. The approach was able to enhance the vertical performance of the localization. A non-real-time approach for historical movement data collection based on barometric measurements was used by [24]. They focused on the localization of human activity based on distinctive altitude patterns in urban areas. The activity patterns were thereby classified as transportation, indoor movement, or outdoor physical activity using a Restricted Boltzmann Machine, which was then solved using Markov Chain Monte Carlo approximation to cluster the activities by their distinctive altitude patterns. Due to the dependence on these patterns, the method is not applicable in outdoor localization tasks of mobile machines. A method to use 3D-track data together with a smartphone internal IMU and barometer for localization tracking in mountain roads was proposed by [25]. A Hidden Markov Model was solved by a Viterbi Algorithm to identify the most probable localization state of the user. The algorithm is based on the definition of a limited amount of slopes and road conditions. [25] In [26], another method of path-based barometric localization has been developed. It is focused on a centralized tracking approach, where the data handling occurs on a remote server, downloading the relevant street maps based on the current IP location and augmenting the map using elevation data from the Google Elevation API. Due to the fact that this approach focuses on not collecting speed data, a dynamic time wrapping algorithm is used to find the similarity between measured altitude and map heights. To identify the current path, they then compare a variety of path finding algorithms. This method is therefore also limited on the usage with specified road maps and not usable in off-road applications.

Our paper proposes a new method of localization by fusing the information generated by a pressure sensor and an altitude map for real-time outdoor applications. The pressure sensor thereby allows the calculation of the altitude of the vehicle. Sequential importance sampling is used in a particle filter to estimate the position of the vehicle by fusing the measured altitude with a surface profile. The filter converges to the real position after a certain amount of consecutive measurements.

The structure of this paper is defined as follows. First, in Section II, the theoretical background of the proposed localization approach is presented. In the subsequent Section III, the experimental setup of the tractor and the GNSS reference are presented. The results and the position accuracy are presented and discussed in Section IV. Section V concludes the paper and discusses open points and future research.

II. Theoretic background

A. Altitude Calculation

The calculation of the altitude from pressure measurements is based on the international height formula. This formula assumes a standard atmospheric composition of 288.15 K with an air pressure level of $p_0 = 1013.25\ hPa$ at sea level and a temperature gradient of 0.65 K/m. Using these assumptions, the altitude can be calculated relative to sea level following [27] given the pressure measurement $p(h)$ as

$$h = \frac{288.15\ K}{0.0065\ \frac{K}{m}} \cdot \left(1 - \left(\frac{p(h)}{p_0}\right)^{\frac{1}{5.255}}\right). \tag{1}$$

The initial altitude level has to be calibrated to minimize the impact of weather and ambient temperature on the measurements. Given the measured pressure $p(h_0)$ at a known height h_0 the corresponding reference pressure p_0 is calibrated following (1) as

$$p_0 = p(h_0) \cdot \left(1 - h_0 \cdot \frac{0.0065\ \frac{K}{m}}{288.15\ K}\right)^{-5.255}. \tag{2}$$

The influence of ambient pressure and temperature changes during one run is neglected.

B. System and filter design

The vehicle is modeled as a discrete-time non-linear time-variant stochastic dynamic system with state $\underline{x}_k$ and time index k. The state vector has four dimensions $\underline{x} = [x, y, v, \theta]$ where x, y are the corresponding coordinates of the projected position in the local coordinate system, v the speed of the vehicle and the current direction of movement θ. The system state at the next time-step $k+1$ is predicted by the transition function $f_k(\underline{x}_k, \underline{\omega}_k)$, with the normal distributed system noise $\underline{\omega}_k$ and the time interval dt as

$$\underline{x}_{k+1} = f_k(\underline{x}_k, \underline{\omega}_k) = \begin{bmatrix} x_k + sin(\theta_k)v_k dt + \omega_{x,k} \\ y_k + cos(\theta_k)v_k dt + \omega_{y,k} \\ v_k + \omega_{v,k} \\ \theta_k + \omega_{\theta,k} \end{bmatrix} \tag{3}$$

The state transition is strongly simplified and does not consider any vehicle properties. Thus, the resulting system can be used for any moving object. The time index k is omitted in the following when inferable from the context.

The system state $\underline{x}_k$ is observed by measurement of the altitude z_k^h, the vehicle speed z_k^v and the vehicle heading z_k^θ. The non-linear measurement function is given as

$$\underline{z}_k = \begin{bmatrix} z_k^h \\ z_k^v \\ z_k^\theta \end{bmatrix} = h(\underline{x}_k, \underline{\nu}_k)$$

with measurement noise $\underline{\nu}_k$.

For a given state vector $\underline{x}_k$, $h(\underline{x}_k, \underline{\nu}_k)$ calculates the height by linear-interpolating the altitude between the nearest raster coordinates of a grid-based surface map. The state estimation is updated by the probability function $p(\underline{z}_k|\underline{x}_k)$ after each measurement which are fused according to Bayes' law [28], following

$$p(\underline{x}_k|\underline{z}_{1:k}) \propto \frac{p(\underline{z}_k|\underline{x}_k)p(\underline{x}_k|\underline{z}_{1:k-1})}{p(\underline{z}_k|\underline{z}_{1:k-1})}. \quad (4)$$

A discrete Dirac-Mixture distribution is used to represent the probability density function $p(\underline{x}_k|\underline{z}_{1:k})$ of the state $\underline{x}_k$ as

$$\hat{p}(\underline{x}_k|\underline{z}_{1:k}) = \sum_{j=1}^{n} w_j \delta(\underline{x}_k - \underline{x}^j),$$

with weights

$$w_j \propto \frac{p(\underline{x}_k|\underline{z}_{1:k})}{q(\underline{x}_k)}$$

and the proposal distribution $q(\underline{x}_k)$ from which the sample set $\mathcal{X} = \underline{x}^j, w^j; j \in [1, N]$ of N samples $\underline{x}^j$ with corresponding weights w^j is drawn.

The measurement noise $\underline{\nu}_k$ is assumed to be normally distributed with covariance $\sum = [diag(\underline{\nu}_k)^2]$ and the weights are updated each time step by

$$w_{k+1}^j = w_k^j \cdot \frac{1}{\sqrt{(2\pi)^p \det(\sum)}} e^{-\frac{1}{2}(h(\underline{x}_k^j) - \underline{z}_k)^T \sum^{-1} (h(\underline{x}_k^j) - \underline{z}_k)}. \quad (5)$$

When working with low noise sensors which directly measure speed and heading, see Section III, the measurements can be assumed to be noise-free to reduce the dimension of the state vector. In this case, the speed v and heading θ are measured by a linear measurement function as

$$z_k^v = v_k$$
$$z_k^\theta = \theta_k$$

This simplification reduces the required amount of particles significantly. v and θ are directly known from the measurements and can be omitted from the state vector, which reduces to the x, y coordinates. In consequence, the measurement $\underline{z}_k$ simplifies to z_k^h and the update function is

$$w_{k+1}^j = w_k^j \cdot \frac{1}{\sqrt{2\pi(\nu_k^h)^2}} e^{-\frac{(h(\underline{x}_k^j) - \underline{z}_k)^2}{2\pi(\nu_k^h)^2}}. \quad (6)$$

The initialization of the filter and the proposal distribution $q(x_k)$ are described in the experimental setup Section III. To avoid weight degeneracy residual re-sampling is used, being described in [29]. A re-sampling step is performed when the effective number of particles as

$$\hat{N}_{eff} = \frac{1}{\sum (w_k^j)^2} < \hat{N}_{th}$$

falls below a threshold $\hat{N}_{th}$.

C. Map based altitude lookup

The core of the algorithm is the fusion of altitude measurements with a-prior knowledge of the altitude. The algorithm uses the grid-based digital terrain model of the ´German Federal Agency for Cartography and Geodesy´[1]. The used terrain model provides altitude data with an accuracy of 0.1 to 1 m in a regular grid. The grid is projected to UTM32 and uses the European Terrestrial Reference System 1989 (ETRS89) with a reference plane for the normal height (DHHN92). The grid data is accessed and converted to Python arrays by GDAL library [30] and modified code based on the Open Elevation API [31]. For a position in UTM32 coordinates $\underline{x} = [x, y]$ the altitude matrix

$$\mathbf{H} = \begin{bmatrix} h_{0,0} & \dots & h_{0,i} \\ \vdots & \ddots & \vdots \\ h_{j,0} & \dots & h_{j,i} \end{bmatrix}$$

is provided with the transform and scaling factors ax,ay,bx,by to calculate the corresponding matrix indices i,j as

$$\hat{i} = (x - ax) \cdot bx$$
$$\hat{j} = (y - ay) \cdot by.$$

In most cases $\hat{i}$ is a floating point figure situated between the positive integer raster indices $\lfloor i_l \rfloor$ and $\lceil i_u \rceil$, ($\hat{j}$ accordingly). The altitude value at the given position $\underline{x}$ is interpolated by a convex hull between the four neighbouring points $\lfloor i_l \rfloor$, $\lceil i_u \rceil$, $\lfloor j_l \rfloor$ and $\lceil j_u \rceil$. [32] provides a open source library for computation of the convex hull.

III. Experimental Setup

A. Hardware Setup

The test vehicle used for measurement data collection was a Fendt 516 Vario tractor fitted with a connection gateway to a measurement computer running Ubuntu with the Robot Operating System (ROS) [33] as middle-ware for data exchange purposes. This setup allows the interaction with vehicle internal data bus systems to extract measurement data from regularly fitted sensors using a connection to the CAN-bus and the ISOBUS. Furthermore, the machine is fitted with additional sensors such as an additional GNSS-Antenna, an Inertial Measurement Unit (IMU), two separate stereo camera systems, and a laser scanner for surface structure detection. A more detailed description of the experimental setup can be found in [34]. Fig. 1 shows the tractor and implement combination during data collection (here paired with a Horsch Terrano 4 FX cultivator).

[1]Geographic base data: © GeoBasis-DE / BKG (2022)

Fig. 1: Data Collection

The signals used for this paper were provided only by the internal sensor systems and the Xsens MTi-300 IMU. Table I shows the used sensor types, the sensor source and the corresponding units.

TABLE I: Used Sensortypes

Signal	**Unit**	**Source**
Radar Speed	km/h	CAN
Magnetic Heading	deg	CAN
Atmospheric Pressure Level	Pa	IMU

Signals from the ISOBUS were used to control the measurements with the more accurate GNSS+RTK localization. A graphical user interface was created to supervise and automate the data collection process, detecting sensor issues. The collected sensor data streams were saved as rosbags, stored in a database, and then processed using Python scripts.

B. Implementation and Initialisation

The algorithm was implemented in Python and executed in an Ubuntu 20.04 environment. Figure 2 shows the sequential calculation steps at each measurement step. In the update step, the measurements are merged to the digital elevation model (DEM). The DEM defines for each sample, with state vector $\underline{x}^j$, an expected altitude measurement $h(\underline{x}^j) = E[z_k^h]$, see Section II-C. Following (6), the corresponding sample weights are updated accordingly with the measured altitude z_k^h. The map altitude $h(\underline{x}^j)$ and the measured altitude z_k^h are subject to noise. Under the assumption of unbiased normal distributed noise, the combined noise is

$$\mathcal{N}_a(0, \sigma_a^2) + \mathcal{N}_b(0, \sigma_b^2) = \mathcal{N}_f(0, \sigma_a^2 + \sigma_b^2).$$

The variance of the normal distributions depends on the DEM quality and the used barometer, as well as atmospheric and meteorologic perturbation. The predict step follows (3) and the estimated vehicle position $\underline{x}_k^e$ is evaluated at the center of gravity of the state distribution $\hat{p}(\underline{x}_k)$ as

$$\underline{x}_k^e = \left[\frac{1}{\sum_{j=1}^n w_j} \sum_{j=1}^n w_j \underline{x}^j \right]_k .$$

In the experiments, the system and measurement noises are defined as

$$\underline{\omega}_k = [1, 1, 0, 0]$$

$$\underline{\nu}_k = [2, 0, 0].$$

The number of samples is set to $N = 1024$ and the re-sampling threshold is set to $\hat{N}_{th} = 100$.

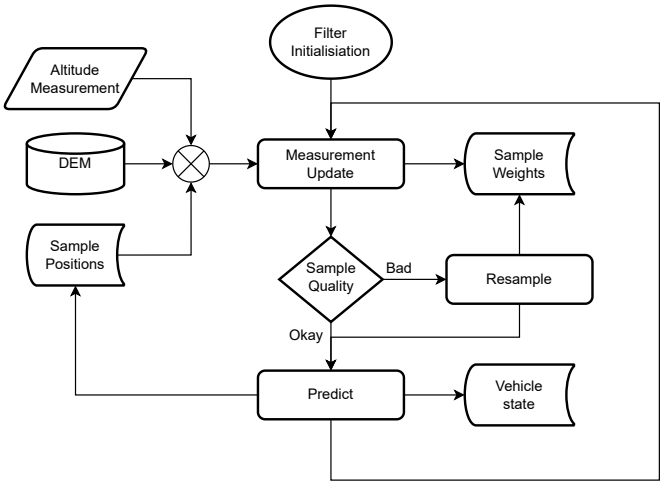

Fig. 2: Calculation steps of the sequentially Monte-Carlo algorithm

At the beginning of each run, the filter is initialized under the assumption that the position of the vehicle is only roughly known to be inside a certain area. An area of 400 to 400 meters is used as the typical extent of the regarded crop fields in our test runs. The window is located at the overall mean position of the run and the samples are drawn as a regular grid inside this area. This initialization of the filter separates each run into two parts. At first, the proposed method is the localization of the vehicle inside the given area. In the second part of each run, after having converged to the current vehicle position, the method acts as a real-time tracker of the moving vehicle.

C. Field tests

The presented algorithm was tested with the described setup at 6 different locations (fields). The parameters of each field are described in Table II. At the beginning of each track the barometer was calibrated at a reference position with a known height (see (2)). Each track was driven only once and for each of the five virtual runs of the algorithm (see Section IV) the same measurements were used.

IV. Results and Discussion

A. Experimental Results

Fig. 3a shows the initialization of the filter and the drawn samples in a regular grid in the area. Fig. 3b and 3c show the evolution of the represented distribution after a 10 and 100 consecutive measurement steps with 4 measurements per seconds. After a few measurements, there are still a couple of possible vehicle positions fitting to the sensed altitude profile.

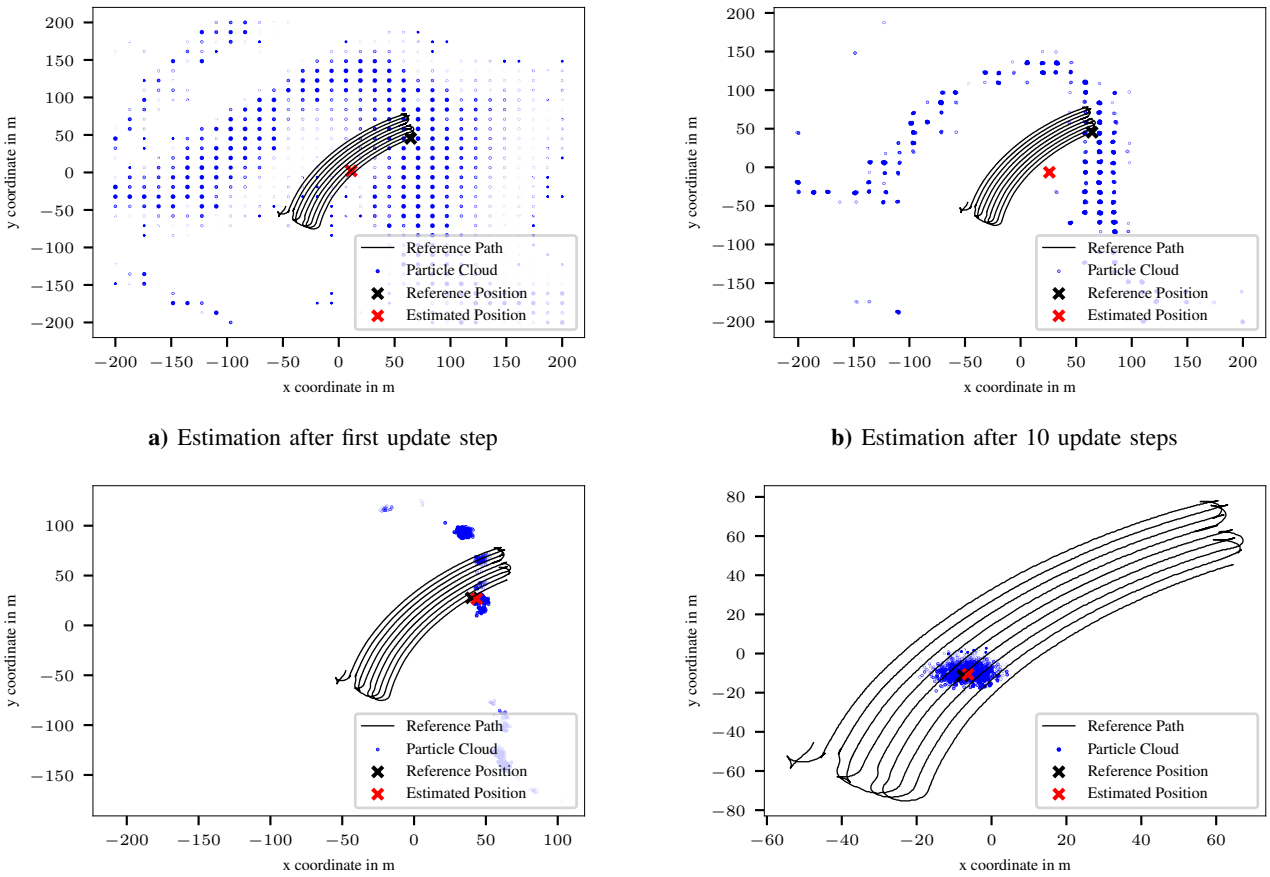

a) Estimation after first update step

b) Estimation after 10 update steps

c) Estimation after 100 update steps

d) Estimation after 500 update steps

Fig. 3: Particle cloud (blue), estimated system state (red) and vehicle reference path and position (black) of field 6, run 1

TABLE II: Field parameters: track length, maximal-, minimal altitude (AMSL) and average surface gradient

No.	Length (m)	Max. Alt. (m)	Min. Alt. (m)	Gradient (%)
1	897	211.7	221.9	6.1
2	1256	187.3	198.8	6.7
3	1497	188.9	195.5	4.6
4	766	197.1	212.1	6.5
5	3651	187.3	198.6	3.6
6	1651	183.3	198.2	8.0

With ongoing measurements, the possible positions decrease until the filter fixes on the vehicle position in Fig. 3d. The uncertainty of the state estimation largely depends on the altitude profile around the vehicle position.

The distance between the estimated position and the reference position is shown as absolute error in Fig. 4 for two exemplary runs of fields 3 and 4. At initialization, the estimated position error is up to 100 m. After less than 50 m, the deviation drops under 5-10 meters with a few peaks. Some peaks with a higher deviation can be observed, e.g. during turning maneuver of the vehicle where dead reckoning is leading to high inaccuracy. However, the error is reducing back to its previous level with ongoing altitude measurements. In Fig. 5 the measured altitude is compared to map altitude at the reference position. The error of the height measurement is up to 2 m with a standard deviation of 0.3 to 0.7 m depending on the field. The measurement noise of the barometer and the difference between the barometer and the map altitude can be identified as one of the most important parameters in terms to improve localization accuracy.

Fig. 6 shows the mean and standard deviation of all six used fields over five random runs of the estimator with the same input measurements. The first 100m of the runs before the fix on the vehicle position were excluded from the evaluation. For all fields, the standard deviation was in the range of 3 to 9 meters, with low variation between individual filter runs. Fields 1 and 4 have an increased overall position error. High maximum errors led to an increased standard deviation in field 1, whereas in field 4, the overall accuracy was lower than in other runs. In both fields, the surface gradient is similar to the other fields, and the most probable cause of the increased deviations is the small field size involving complex turning maneuvers. Because both runs have not be repeated on different days, potential calibration or environmental effects on

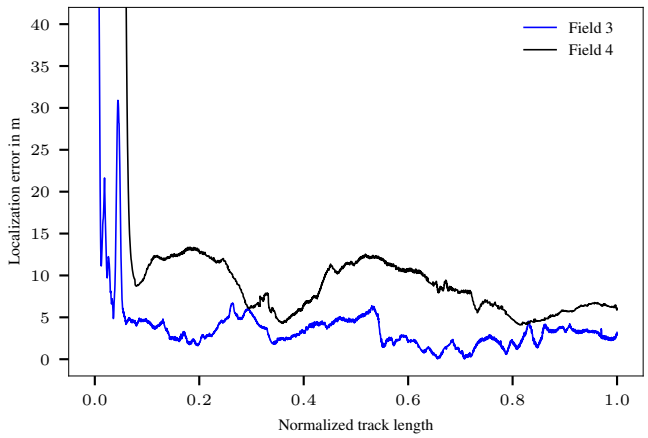

Fig. 4: Temporal Progression of the absolute localization error for two exemplary runs.

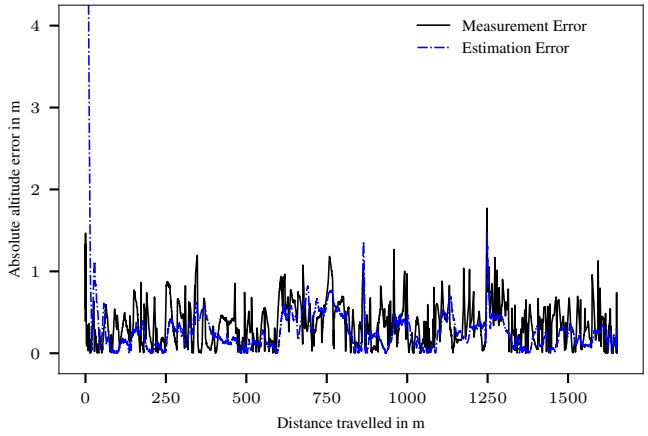

Fig. 5: Deviation between the measured and map altitude at given reference position (Measured Deviation), as well as the deviation at the estimated position (Estimator Deviation) (field 6)

the pressure measurements cannot be ruled out.

B. Discussion

At all 6 test fields, the presented algorithm was able to estimate the correct vehicle position after 100 m. This high reliability comes, however, at a certain expense regarding tracking accuracy. As remarked in Fig. 5, the altitude measurements show a standard deviation of up to 0.7 m. The filter, on the contrary, is implemented with an assumed noise variance of 4 m. The increased noise is needed because of the low number of samples. Assuming an unknown vehicle position, the samples are initialized in a regular grid, and each row of 400 m consists of only 32 samples, leading to a spatial distance of 12.5 m between samples in this grid. Forcing a low noise on the altitude measurements leads to a possible dead-lock of the filter when no sample is situated at the exact vehicle position after initialization. The same effect, although less severe, appears during turning maneuvers when dead reckoning leads to high position deviations. For optimal tracking results, the vehicle motion model should be adapted and the measurements noise could then be decreased.

In this paper, to demonstrate the proposed method independently of a specific vehicle, a simple motion model was used. Integrating the speed and heading measurements into the estimator is quite challenging, as both are changing rapidly during the operation of the vehicle due to control input. It is not recommended to model the vehicle's behavior changes caused by the driver control input as system noise, as a high system noise is needed to adapt quickly to the new system state which leads to decreased filter performance. On the contrary, using a sophisticated vehicle model, taking the driver input into account, could significantly improve the performance of the estimator.

The resulting localization accuracy is not sufficient to provide an alternative to RTK- or D-GPS systems. However, an accuracy in the range of 5 to 10 m is of the same magnitude as conventional GNSS systems without correction signals. The localization method focuses on two main use cases. In combination with other localization systems (e.g. Scan-Matching), it can provide robust localization in areas where GNSS-accuracy is limited, e.g. inside forests. Alternatively, it offers a redundancy and fall-back system for GNSS-based localization in the case of GNSS failure, failure of correction signals, or intentional GNSS jamming attacks.

It is obvious, that the presented algorithm is unable to track the position of the vehicle without a surface gradient. When comparing the surface gradient with the estimator accuracy in Fig. 6 no direct connection between average surface gradient and estimator accuracy is remarked. In Field 3 an average surface gradient of 4.6 % was already sufficient for a tracking accuracy of 3m and a position fix in less than 100 m, corresponding to ca. 5 m of altitude difference. A surface gradient of 5 % is not unusual in many outdoor applications and offers a high range of possible applications for the presented method.

V. Conclusion

In this paper, we presented a new method for localization and real-time tracking of vehicles in off-road scenarios. A particle filter was designed using sequential importance sampling for estimating the vehicle position based on the non-linear altitude measurement. The relative vehicle motion was predicted by a simple vehicle model that is applicable to a wide range of vehicles. The current altitude at the vehicle position was measured with a barometric pressure sensor. In the update function, the map altitude at each sample position was compared to the measurement, and the filter weights were updated accordingly. The algorithm works with an offline map and does not require any additional infrastructure, nor does it rely on any exterior real-time data.

The algorithm was evaluated on test drives using a Fendt 516 Vario equipped with an additional barometer for measuring the atmospheric pressure. The evaluation of each test drive has been separated into two parts. At first, the vehicle's

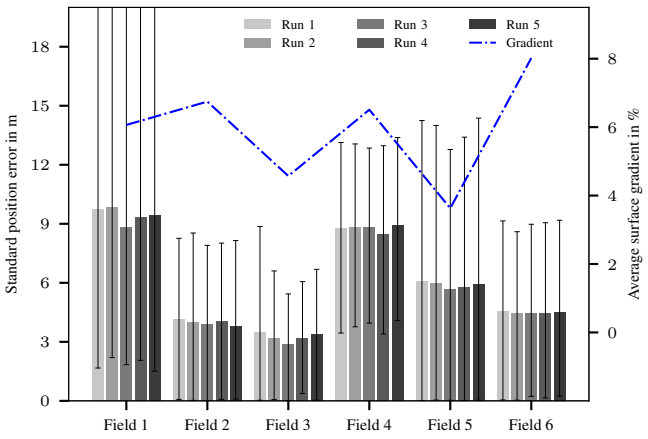

Fig. 6: Estimation error over 5 random runs (primary y-axis) and average surface gradient (secondary y-axis) of all 6 field tests

position was limited to a certain area of 400 m to 400 m in which the filter was initialized. During the first 100 m of the vehicle's track, the algorithm was able to fix the vehicle's position. In the second part, the algorithms' abilities for real-time tracking were evaluated, showing a standard deviation of less than 10 m. In the experiments, the algorithm showed high robustness and reliability in the tested locations. Although altitude-based localization cannot be carried out in completely flat areas, surface gradients of 3-4 % are already sufficient for localization. The algorithm could offer a redundancy and alternative to GNSS systems in mountainous areas.

Besides its proven accuracy, there are several possible improvements and additions to the proposed algorithms that are conceivable. The algorithm does not need any particular vehicle model. However, an adapted vehicle model that considers steering angle, vehicle kinematics, brake and acceleration commands, is expected to further improve the results. The experiments in this paper were conducted in an agricultural environment where highly accurate speed and reference position measurements are possible. This allows a clear evaluation of the algorithms' performance. However, further experiments should be performed to evaluate it in areas where GNSS-accuracy is limited, e.g. in forest environments.

References

[1] X. Zhang, M. Geimer, P. O. Noack, and M. Ehrl, "Elektronische Deichsel für landwirtschaftliche Arbeitsmaschine - Auf dem Weg nach autonomen Landmaschinen," *LAND.TECHNIK 2010 Tagungsband. 68. Internationale Tagung. 27./28. Oktober 2010, Braunschweig*, 2010.

[2] M. Perez-Ruiz and S. K., "GNSS in Precision Agricultural Operations," in *New Approach of Indoor and Outdoor Localization Systems* (F. Elbahhar, ed.), InTech, Oct. 2012.

[3] C. Geiger, S. Beiser, and M. Geimer, "Automated Driving on a Skid Road with a Forwarder in a CTL Logging Process," in *Proceedings of The Joint 43rd Annual Meeting of Council on Forest Engineering (COFE) & the 53rd International Symposium on Forest Mechanization (FORMEC), Forest Engineering Family – Growing Forward Together, September 27-30, 2021, Corvallis, Oregon, U.S.A. Ed.: W. Chung*, p. 135, 2021.

[4] R. Karlsson and F. Gustafsson, "The Future of Automotive Localization Algorithms: Available, reliable, and scalable localization: Anywhere and anytime," *IEEE Signal Processing Magazine*, vol. 34, pp. 60–69, Mar. 2017. Conference Name: IEEE Signal Processing Magazine.

[5] A. Schlichting and C. Brenner, "Localization using automotive laser scanners and local pattern matching," in *2014 IEEE Intelligent Vehicles Symposium Proceedings*, pp. 414–419, June 2014. ISSN: 1931-0587.

[6] M. Geimer, *Mobile working machines*. Warrendale, Pennsylvania (USA): SAE International, 2020. doi: 10.4271/9780768094329.

[7] J. B. Harley and D. Woodward, eds., *Cartography in prehistoric, ancient, and medieval Europe and the Mediterranean*. No. v. 1 in The history of cartography, Chicago: University of Chicago Press, 1987.

[8] A. J. Kent and A. Hopfstock, "Topographic Mapping: Past, Present and Future," *The Cartographic Journal*, vol. 55, pp. 305–308, Oct. 2018. Publisher: Taylor & Francis _eprint: https://doi.org/10.1080/00087041.2018.1576973.

[9] W. E. K. Middleton, *The history of the barometer*. 1964.

[10] S. Lo, "Navigation for Aviation," in *Position, Navigation, and Timing Technologies in the 21st Century* (Y. T. J. Morton, F. Diggelen, J. J. Spilker, B. W. Parkinson, S. Lo, and G. Gao, eds.), pp. 1871–1891, Wiley, 1 ed., Dec. 2020.

[11] D. J. Jacob, *Introduction to Atmospheric Chemistry*. Princeton University Press, 1999. Google-Books-ID: FcqHAQAACAAJ.

[12] J. M. Rüeger, *Electronic Distance Measurement*. Berlin, Heidelberg: Springer Berlin Heidelberg, 1996.

[13] S. Gaglione, A. Angrisano, G. Castaldo, C. Gioia, A. Innac, L. Perrotta, G. Del Core, and S. Troisi, "GPS/Barometer augmented navigation system: Integration and integrity monitoring," in *2015 IEEE Metrology for Aerospace (MetroAeroSpace)*, pp. 166–171, June 2015.

[14] H. Qin, H. Zhang, Y. Niu, X. Chen, and S. Zhang, "Altitude data fusion algorithm based on INS and GNSS and barometer," in *2021 IEEE 3rd International Conference on Civil Aviation Safety and Information Technology (ICCASIT)*, pp. 85–90, Oct. 2021.

[15] B. Li, B. Harvey, and T. Gallagher, "Using barometers to determine the height for indoor positioning," in *International Conference on Indoor Positioning and Indoor Navigation*, pp. 1–7, Oct. 2013.

[16] H. Ye, T. Gu, X. Tao, and J. Lu, "B-Loc: Scalable Floor Localization Using Barometer on Smartphone," in *2014 IEEE 11th International Conference on Mobile Ad Hoc and Sensor Systems*, pp. 127–135, Oct. 2014. ISSN: 2155-6814.

[17] C. Ruan, M. Yu, X. He, and B. Song, "An Indoor Floor Positioning Method Based on Smartphone's Barometer," in *2018 Ubiquitous Positioning, Indoor Navigation and Location-Based Services (UPINLBS)*, pp. 1–9, Mar. 2018.

[18] X. Shen, Y. Chen, J. Zhang, L. Wang, G. Dai, and T. He, "BarFi: Barometer-Aided Wi-Fi Floor Localization Using Crowdsourcing," in *2015 IEEE 12th International Conference on Mobile Ad Hoc and Sensor Systems*, pp. 416–424, Oct. 2015.

[19] J. Ying, C. Ren, and K. Pahlavan, "A barometer-assisted method to evaluate 3D patient geolocation inside hospital," in *2016 10th International Symposium on Medical Information and Communication Technology (ISMICT)*, pp. 1–4, Mar. 2016. ISSN: 2326-8301.

[20] Z. Xu, J. Wei, J. Zhu, and W. Yang, "A robust floor localization method using inertial and barometer measurements," in *2017 International Conference on Indoor Positioning and Indoor Navigation (IPIN)*, pp. 1–8, Sept. 2017. ISSN: 2471-917X.

[21] Y. Zhao, J. Liang, X. Sha, J. Yu, H. Duan, G. Shi, and W. J. Li, "Estimation of Pedestrian Altitude Inside a Multi-Story Building Using an Integrated Micro-IMU and Barometer Device," *IEEE Access*, vol. 7, pp. 84680–84689, 2019. Conference Name: IEEE Access.

[22] Y. Son and S. Oh, "A barometer-IMU fusion method for vertical velocity and height estimation," in *2015 IEEE SENSORS*, pp. 1–4, Nov. 2015.

[23] J. Zhang, E. Edwan, J. Zhou, W. Chai, and O. Loffeld, "Performance investigation of barometer aided GPS/MEMS-IMU integration," in *Proceedings of the 2012 IEEE/ION Position, Location and Navigation Symposium*, pp. 598–604, Apr. 2012. ISSN: 2153-3598.

[24] H. Ye, L. Sheng, T. Gu, and Z. Huang, "SELoc: Collect Your Location Data Using Only a Barometer Sensor," *IEEE Access*, vol. 7, pp. 88705–88717, 2019. Conference Name: IEEE Access.

[25] H. Ye, W. Yang, Y. Yao, T. Gu, and Z. Huang, "BTrack: Using Barometer for Energy Efficient Location Tracking on Mountain Roads," *IEEE Access*, vol. 6, pp. 66998–67009, 2018. Conference Name: IEEE Access.

[26] B.-J. Ho, P. Martin, P. Swaminathan, and M. Srivastava, "From Pressure to Path: Barometer-based Vehicle Tracking," in *Proceedings of the*

2nd ACM International Conference on Embedded Systems for Energy-Efficient Built Environments, BuildSys '15, (New York, NY, USA), pp. 65–74, Association for Computing Machinery, Nov. 2015.

[27] D. E. Bolanakis, K. T. Kotsis, and T. Laopoulos, "Temperature influence on differential barometric altitude measurements," in *2015 IEEE 8th International Conference on Intelligent Data Acquisition and Advanced Computing Systems: Technology and Applications (IDAACS)*, vol. 1, pp. 120–124, Sept. 2015.

[28] M. Arulampalam, S. Maskell, N. Gordon, and T. Clapp, "A tutorial on particle filters for online nonlinear/non-Gaussian Bayesian tracking," *IEEE Transactions on Signal Processing*, vol. 50, pp. 174–188, Feb. 2002.

[29] R. Douc and O. Cappe, "Comparison of resampling schemes for particle filtering," in *ISPA 2005. Proceedings of the 4th International Symposium on Image and Signal Processing and Analysis, 2005.*, pp. 64–69, Sept. 2005.

[30] E. Rouault, F. Warmerdam, K. Schwehr, A. Kiselev, H. Butler, and M. Łoskot, "GDAL." Zenodo, Jan. 2022.

[31] J. R. Lourenço, "Open-Elevation," Feb. 2022.

[32] "Qhull code for Convex Hull, Delaunay Triangulation, Voronoi Diagram, and Halfspace Intersection about a Point." http://www.qhull.org/.

[33] A. Koubaa, ed., *Robot Operating System (ROS)*, vol. 625 of *Studies in Computational Intelligence*. Cham: Springer International Publishing, 2016.

[34] S. Becker, K. Daiss, K. Daaboul, M. Geimer, and M. J. Zöllner, "Machine Learning for Process Automation of Mobile Machines in Field Applications," in *Land.Technik AgEng 2019 : Hannover, Nov. 8th + 9th 2019 : 77th International Conference on Agricultural Engineering*, p. 187, 2019. ISSN: 0083-5560.